A Novel Tailsitter UAV with Configurable Wings

Yoshinaga, Shunsuke
Graduate School and Faculty of Information Science and Electrical Engineering, Kyushu University

Sakaguchi, Akinori
Graduate School and Faculty of Information Science and Electrical Engineering, Kyushu University

Yamamoto, Kaoru
Graduate School and Faculty of Information Science and Electrical Engineering, Kyushu University

出版情報：Journal of Robotics and Mechatronics. 36 (5), pp.1037-1042, 2024-10-20. 富士技術出版株式会社
バージョン：

https://doi.org/10.20965/jrm.2024.p1037

Paper:

A Novel Tailsitter UAV with Configurable Wings

Shunsuke Yoshinaga[‡]**, Akinori Sakaguchi**[‡,†]**, and Kaoru Yamamoto**

Graduate School and Faculty of Information Science and Electrical Engineering, Kyushu University
744 Motooka, Nishi-ku, Fukuoka, Fukuoka 819-0395, Japan
E-mail: {yoshinaga.shunsuke.207@s., sakaguchi@ees., yamamoto@ees.}kyushu-u.ac.jp
[†]Corresponding author
[Received December 15, 2023; accepted March 4, 2024]

In this study, we propose a novel tailsitter unmanned aerial vehicle with configurable wings using a parallel link mechanism. It has two flight modes: a hover mode and a forward flight mode by pitching, similar to conventional tailsitters. In addition, it can deform its airframe in each flight mode. In the hover mode, it can tilt the frame in the pitch direction while hovering. In the forward flight mode, it can change the configuration of the wings during forward flight. In experiments, we show that it can transition from the hover mode to the forward flight mode with three wing configurations: non-staggered wings (biplane) and positively and negatively staggered wings (tandem wing plane), using an attitude controller for conventional quadrotors.

(a) Hover mode (b) Forward flight mode

Fig. 1. Proposed tailsitter with configurable wings where figures (a) and (b) show the hover and forward flight states, respectively.

Keywords: tailsitter, configurable wing, parallel link mechanism

1. Introduction

Quadrotors have emerged as versatile tools across numerous fields, including logistics, inspection, surveying, and aerial photography. However, their underactuated nature limits their ability to control their position and attitude independently. One solution to this problem is a non-planar multirotor [1], achieved by increasing the number of rotors and tilting the rotor surfaces in relation to the body. Unfortunately, this results in lower flight efficiency due to the increased weight and the thrust loss.

In response to these challenges, deformable quadrotors have gained significant attention due to their enhanced flexibility. For instance, in our previous work, we introduced a quadrotor capable of tilting its frame in the pitch direction while hovering [2]. This capability is particularly advantageous for tasks requiring precise maneuvering in confined spaces, allowing the quadrotor to narrow its width to almost as little as one rotor diameter. Additionally, it facilitates inspections along curved surfaces, such as tunnels, by dynamically adjusting the tilt angle of the frame to match the surface curvature.

Among the variety of deformable quadrotors with tilting mechanisms—ranging from tilting rotor types [3–7] to tilting arm [8–10] and frame types [2, 11, 12]—our quadrotor offers several advantages provided by its unique parallel link mechanism. Firstly, it requires only one additional actuator for tilting. Secondly, all rotor surfaces remain parallel at any state. This design ensures a similar hovering efficiency to conventional quadrotors (i.e., those without deformation capability). In contrast, many quadrotors with tilting mechanisms often suffer from increased weight due to multiple additional actuators or thrust loss caused by non-parallel rotor surfaces.

Motivated by these advantages, we propose a novel tailsitter unmanned aerial vehicle (UAV) with configurable wings using the parallel link mechanism (see **Fig. 1**) similar to the one in [2]. The particular focus here is to improve the forward flight efficiency while retaining all the advantages of [2] during hovering. Specifically, we maintain the basic structure of the quadrotor in [2] and add two wings in such a way that it can smoothly switch between hover and forward flight modes by pitching, similar to conventional tailsitter UAVs [13–15]. In the hover mode, it behaves like the quadrotor with a tilting frame [2]. In the forward flight mode, it functions as a configurable-wing UAV that moves forward using the lift generated by the upper and lower wings, similar to conventional fixed-wing UAVs. In addition, it can change the configuration of the two wings while maintaining wing parallelism during forward flight. Compared to existing UAVs with similar features, such as the VTOL aircraft tilt-wing UAV [16], the proposed tailsitter benefits from better weight efficiency and maintenance due to the addition of only one actuator.

The main contributions of this paper can be summarized

1. The authors with ‡ mark contributed equally to this research.

as follows. Firstly, we introduce the concept of a novel tailsitter UAV featuring a parallel link mechanism and configurable wings. Secondly, we present a prototype aimed at testing its ability to seamlessly transition between the hover and forward flight modes, while ensuring that the attached wings do not interfere with the tilting frame. For this purpose, we employ rectangular flat plate wings for their mechanical simplicity and ease of manufacture. However, it is worth noting that the proposed tailsitter UAV falls within the low Reynolds number range of 10^4 to 10^5. In this range, thin cambered plate airfoils yield higher lift coefficients compared to flat plate airfoils [17]. The investigation of the optimal airfoil shape is left as future work.

The remainder of this paper is organized as follows. In Section 2, we explain the mechanism of the proposed tailsitter UAV with configurable wings and its flight mode with deformations, and present its prototype. Section 3 describes the control architecture for a stable flight in the two flight modes. In Section 4, we demonstrate that it can transition between two flight modes with three wing configurations. Finally, the conclusion is presented in Section 5.

2. Mechanism

In this section, we first provide an overview of our proposed tailsitter UAV with configurable wings using a parallel link mechanism. Next, we describe in detail the two flight modes generated by pitching and the deformation mechanism in each flight mode. Finally, we show a prototype of our proposed tailsitter.

2.1. Proposed Tailsitter UAV

Figure 2 shows a mechanical model of the proposed tailsitter UAV. It has basically the same structure as the quadrotor UAV developed in our previous work [2]. The difference lies in the presence of two wings. It mainly consists of a body, tilting frames, and additional wings. The body is equipped with a flight computer, a LiPo battery, and one servo motor, which are stacked in the $e_z^{\mathcal{B}}$-axis direction of the body-fixed frame to reduce aerodynamic drag as a tailsitter. The tilting frame consists of upper and lower E-shaped frames, where the central and end parts of these frames are connected by the body and two arms, respectively. These frames incorporate bearings to form a parallel link, and the central fulcrum of the upper frame is driven directly by the servo motor mounted on the body. When driven by the servo motor, the entire frame tilts around the $e_y^{\mathcal{B}}$-axis due to the parallel link mechanism, as shown in **Fig. 2(b)**. The angle between the frame and the $e_x^{\mathcal{B}}$-axis, referred to as the tilt angle, is denoted as γ. The important point is that the parallel relation among the body, the front arm, and the rear arm is guaranteed at any tilt angle $\gamma \in [-\gamma_{\max}, \gamma_{\max}]$, where $\gamma_{\max}$ is the maximum tilt angle. Here, wings (rectangular flat plate wings for simplicity in this study) are added to the front and rear arms in order to gain the advantage of a fixed-wing UAV that is more efficient than a conventional quadrotor in forward flight. This

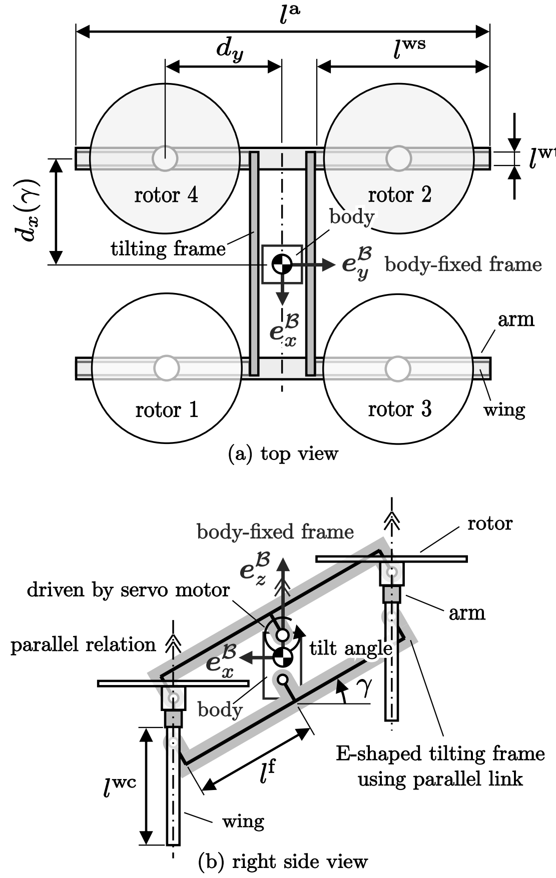

Fig. 2. Mechanical model of the proposed tailsitter UAV.

tailsitter structure obtains two flight modes with deformations, which will be detailed in the next subsection.

2.2. Two Flight Modes with Deformations

With the fuselage structure shown in **Fig. 2**, the proposed UAV can change into various and diverse flight states as shown in **Fig. 3**. First, it has two flight modes: hover mode $\mathcal{M}_{\text{hover}}$ in **Fig. 3(a)** and forward flight mode $\mathcal{M}_{\text{forward}}$ in **Fig. 3(b)**, similar to the conventional tailsitters [13] by the addition of wings. These flight modes are transitioned $\mathcal{M}_{\text{hover}} \rightleftarrows \mathcal{M}_{\text{forward}}$ by pitching, that is, the pitch angle is $\theta \approx 0$ in $\mathcal{M}_{\text{hover}}$ and $\theta \gtrapprox 0$ in $\mathcal{M}_{\text{forward}}$.

Next, it can be deformed into various shapes in each flight mode with only one servo motor. In $\mathcal{M}_{\text{hover}}$, it behaves as a quadrotor UAV with the tilting frame [2]. It hovers at a desired position and yaw angle by adjusting the four rotor thrusts $\boldsymbol{f}_1, \dots, \boldsymbol{f}_4$, similar to conventional quadrotor. Additionally, it can tilt the frame by γ positively and negatively around the $e_y^{\mathcal{B}}$-axis while maintaining rotor parallelism during hover $\theta \approx 0$, as shown in **Fig. 3(a)**. Also, the width of the fuselage in the $e_x^{\mathcal{B}}$-axis direction can be reduced according to the tilting motion of the frame. On the other hand, in $\mathcal{M}_{\text{forward}}$, it behaves as a configurable-wing UAV. It tilts the pitch angle $\theta \gtrapprox 0$, allowing it to move forward using both the propulsion $\boldsymbol{f}_i$ by rotors and the lifts $\boldsymbol{f}_{\text{upper}}$ and $\boldsymbol{f}_{\text{lower}}$ generated by the upper and lower wings. In addition, it can change the configuration of the

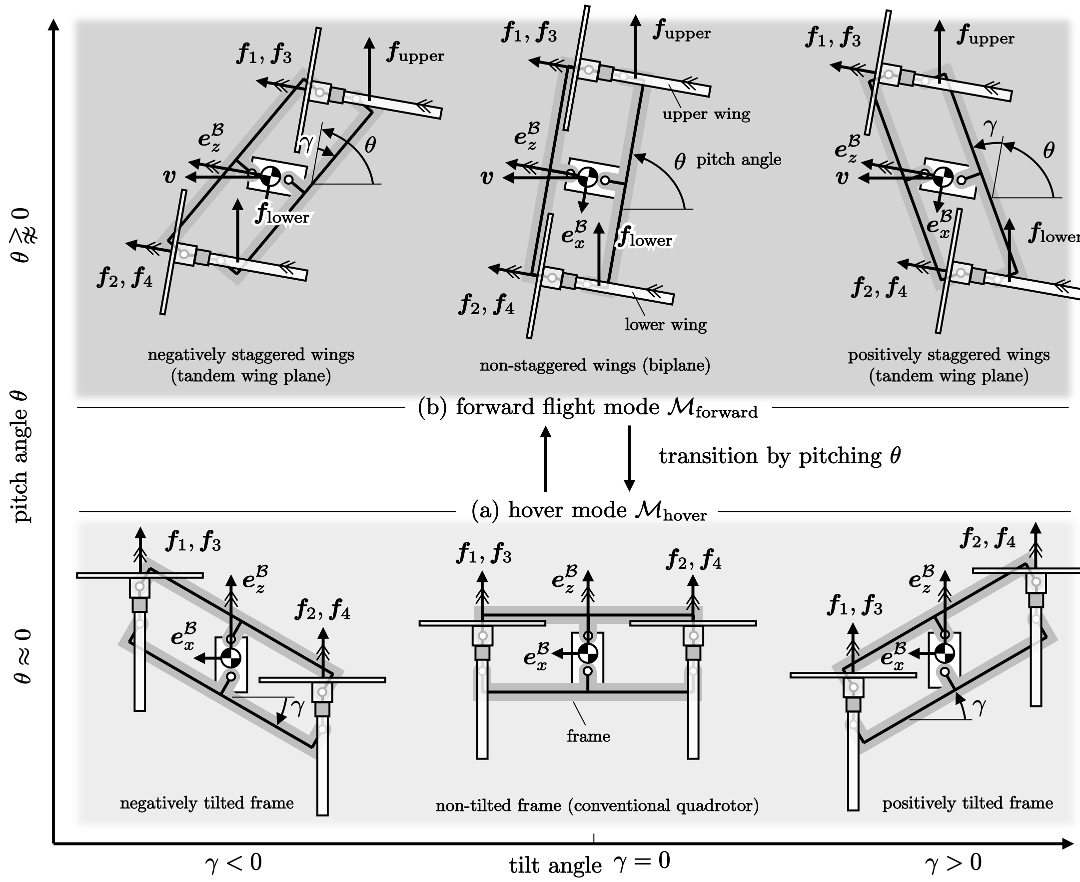

Fig. 3. Two flight modes with deformations and their transitions by pitching.

two wings while maintaining wing parallelism during forward flight. As shown in **Fig. 3(b)**, it can stagger the two wings forward and backward along the $e_z^{\mathcal{B}}$-axis direction, resulting in a biplane at $\gamma = 0$, a tandem wing plane with positively staggered wings in $\gamma > 0$, and a tandem wing plane with negatively staggered wings in $\gamma < 0$.

Finally, it has the same property as the conventional quadrotor in any state with respect to the flight mechanism utilizing the rotor thrust. All rotor thrusts f_i are parallel to the $e_z^{\mathcal{B}}$-axis at any state in both modes $\mathcal{M}_{\text{hover}}$ and $\mathcal{M}_{\text{forward}}$ by the parallel link, that is,

$$f_1 \parallel f_2 \parallel f_3 \parallel f_4 \parallel e_z^{\mathcal{B}}, \ ^\forall\gamma \in [-\gamma_{\max}, \gamma_{\max}]. \quad . \quad . \quad (1)$$

Therefore, total rotor thrust $\sum_i f_i$ is efficiently used to counteract its gravity mg in $\mathcal{M}_{\text{hover}}$ and propel the aircraft forward in $\mathcal{M}_{\text{forward}}$.

2.3. Prototype

Based on the concepts introduced in the previous subsections, we have developed a prototype, as shown in **Fig. 4**. The physical parameters of the prototype and the products employed are listed in **Tables 1** and **2**, respectively. The two arms and tilting frames are made of carbon, while the rectangular flat plate wings are made of styrene boards. The frame dimensions are selected based on the parameters of the tilting frame quadrotor [2]. Note that this prototype operates in the low Reynolds number range of about 10^5, with a chord of 0.1 m and a maximum flight speed of 15 m/s. As mentioned in the introduction, the wing shape chosen for this prototype may not be optimal for this type of aircraft, but is selected for ease of manufacture.

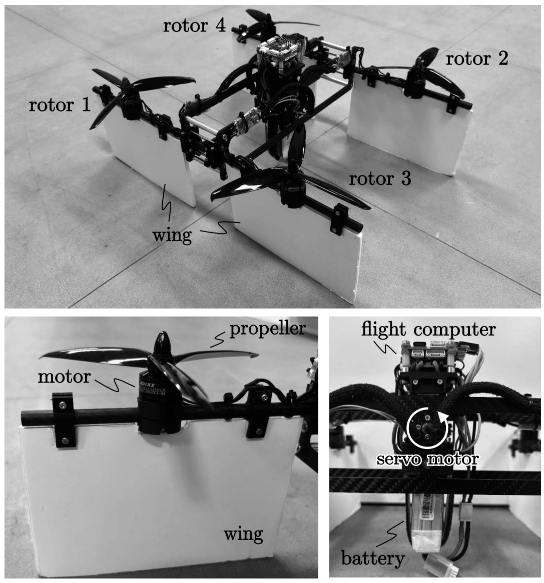

Fig. 4. Prototype of the proposed UAV.

Table 1. Physical parameters of the prototype.

Parameter	Description	Value
m	Mass	596 g
$\gamma_{\max}$	Maximum tilt angle	80°
l^{f}	Tilting frame length	125 mm
l^{a}	Arm length	380 mm
l^{p}	Propeller length	152 mm
l^{wc}	Wing chord	100 mm
l^{ws}	Wing span	160 mm
l^{wt}	Wing thickness	5 mm
κ	Rotor specific thrust-to-drag ratio	1.54×10^{-2} m

Table 2. Products employed in prototype parts.

Parts	Product
Flight computer	mRo PixRacer Pro
Propeller	Gemfan Flash 6042-3
Motor	Emax MT1806 2280KV
ESC	Holybro Tekko32 F4 45A ESC
Servo motor	Kondo KRS-2572R2HV ICS
Power board	Holybro PM06 V2 Power Module
Battery	Tattu 3S 850 mAh 11.1 V
RC radio transmitter	Futaba T10J
RC radio receiver	Futaba R2000SBM

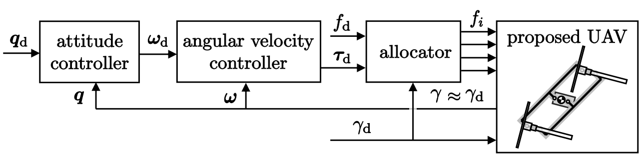

Fig. 5. Control architecture based on conventional quadrotor control method.

3. Control

We show the control architecture in **Fig. 5** that allows the user to stabilize and deform the proposed tailsitter by manual operation. The control system consists of an attitude controller, an angular velocity controller, and an allocator.

The attitude controller is applied to the singularity-free quaternion-based method [18] conventionally used for quadrotors under two conditions: first, all rotors and the flight computer are parallel as in Eq. (1); second, there is a significant change in the pitch angle for mode transitions. The attitude controller generates the desired angular velocity $\boldsymbol{\omega}_{\mathrm{d}}$ from the error quaternion $\boldsymbol{q}_{\mathrm{e}} = \boldsymbol{q}^{-1} \otimes \boldsymbol{q}_{\mathrm{d}} = [q_{\mathrm{e}}\ \tilde{\boldsymbol{q}}_{\mathrm{e}}^{\top}]^{\top}$ between the desired quaternion $\boldsymbol{q}_{\mathrm{d}}$ and the current quaternion $\boldsymbol{q}$ as follows:

$$\boldsymbol{\omega}_{\mathrm{d}} = 2\,\mathrm{sgn}(q_{\mathrm{e}})\,\boldsymbol{K}_{\mathrm{p}}^{\boldsymbol{q}}\tilde{\boldsymbol{q}}_{\mathrm{e}}, \quad \dots \dots \dots \quad (2)$$

where $\boldsymbol{K}_{\mathrm{p}}^{\boldsymbol{q}}$ is the gain matrix for attitude quaternion $\boldsymbol{q}$. q_{e} and $\tilde{\boldsymbol{q}}_{\mathrm{e}}$ are the scalar and vector parts of the error quaternion $\boldsymbol{q}_{\mathrm{e}} = [q_{\mathrm{e}}\ \tilde{\boldsymbol{q}}_{\mathrm{e}}^{\top}]^{\top}$, respectively, and $\mathrm{sgn}(q_{\mathrm{e}})$ is the following sign function of q_{e}.

$$\mathrm{sgn}(q_{\mathrm{e}}) = \begin{cases} 1, & \text{if } q_{\mathrm{e}} \geq 0, \\ -1, & \text{if } q_{\mathrm{e}} < 0. \end{cases} \quad \dots \dots \dots \quad (3)$$

The angular velocity controller is the PID controller that outputs the desired torque $\boldsymbol{\tau}_{\mathrm{d}}$ from the error angular velocity $\boldsymbol{\omega}_{\mathrm{e}} = \boldsymbol{\omega}_{\mathrm{d}} - \boldsymbol{\omega}$.

$$\boldsymbol{\tau}_{\mathrm{d}} = \boldsymbol{K}_{\mathrm{p}}^{\boldsymbol{\omega}}\boldsymbol{\omega}_{\mathrm{e}} + \boldsymbol{K}_{\mathrm{i}}^{\boldsymbol{\omega}} \int \boldsymbol{\omega}_{\mathrm{e}}(\tau)d\tau + \boldsymbol{K}_{\mathrm{d}}^{\boldsymbol{\omega}}\dot{\boldsymbol{\omega}}_{\mathrm{e}}, \quad \dots \quad (4)$$

where $\boldsymbol{K}_{\mathrm{p}}^{\boldsymbol{\omega}}$, $\boldsymbol{K}_{\mathrm{i}}^{\boldsymbol{\omega}}$, and $\boldsymbol{K}_{\mathrm{d}}^{\boldsymbol{\omega}}$ are the proportional gain, integral gain, and derivative gain matrices for the angular velocity, respectively.

The allocator calculates the four rotor thrusts $f_i = \|\boldsymbol{f}_i\|$ $(i = 1, 2, 3, 4)$ from the control inputs of the desired total thrust f_{d} and the desired torque $\boldsymbol{\tau}_{\mathrm{d}}$ as follows:

$$\begin{bmatrix} f_1 \\ f_2 \\ f_3 \\ f_4 \end{bmatrix} = T(\gamma)^{-1} \begin{bmatrix} f_{\mathrm{d}} \\ \boldsymbol{\tau}_{\mathrm{d}} \end{bmatrix}, \quad \dots \dots \dots \quad (5)$$

where $T(\gamma)$ is the following matrix depending on the tilt angle γ.

$$T(\gamma) = \begin{bmatrix} 1 & 1 & 1 & 1 \\ -d_y & d_y & d_y & -d_y \\ -d_x(\gamma) & d_x(\gamma) & -d_x(\gamma) & d_x(\gamma) \\ -\kappa & -\kappa & \kappa & \kappa \end{bmatrix}, \quad \dots \quad (6)$$

where $d_x(\gamma) = l^{\mathrm{f}} \cos\gamma$ and $d_y = l^{\mathrm{f}}$ are the distances between the center of gravity and the rotor in the $\boldsymbol{e}_x^{\mathcal{B}}$- and $\boldsymbol{e}_y^{\mathcal{B}}$-axis directions, respectively. κ is the rotor specific thrust-to-drag ratio. Here, we assume that the tilt angle is close to the desired one, i.e., $\gamma \approx \gamma_{\mathrm{d}}$ because the tilting frame is driven slowly, and therefore we approximate $T(\gamma) \approx T(\gamma_{\mathrm{d}})$. Also, $T(\gamma_{\mathrm{d}})$ is always invertible since the maximum tilt angle is set at 80°, as shown in **Table 1**.

The user can change the proposed tailsitter to the various flight configurations in **Fig. 3** by providing the controller with the desired total thrust f_{d}, the desired attitude $\boldsymbol{q}_{\mathrm{d}}$, and the desired tilt angle γ_{d} appropriately. The relationship between $\boldsymbol{q}_{\mathrm{d}}$ and desired ZYX-Euler angles $\phi_{\mathrm{d}}, \theta_{\mathrm{d}}, \psi_{\mathrm{d}}$ is as follows, and the user specifies $\theta_{\mathrm{d}} \approx 0°$ for $\mathcal{M}_{\mathrm{hover}}$ and $\theta_{\mathrm{d}} \approx 90°$ for $\mathcal{M}_{\mathrm{forward}}$:

$$\boldsymbol{q}_{\mathrm{d}}(\phi_{\mathrm{d}}, \theta_{\mathrm{d}}, \psi_{\mathrm{d}}) = \begin{bmatrix} c\left(\frac{\phi_{\mathrm{d}}}{2}\right)c\left(\frac{\theta_{\mathrm{d}}}{2}\right)c\left(\frac{\psi_{\mathrm{d}}}{2}\right) + s\left(\frac{\phi_{\mathrm{d}}}{2}\right)s\left(\frac{\theta_{\mathrm{d}}}{2}\right)s\left(\frac{\psi_{\mathrm{d}}}{2}\right) \\ s\left(\frac{\phi_{\mathrm{d}}}{2}\right)c\left(\frac{\theta_{\mathrm{d}}}{2}\right)c\left(\frac{\psi_{\mathrm{d}}}{2}\right) - c\left(\frac{\phi_{\mathrm{d}}}{2}\right)s\left(\frac{\theta_{\mathrm{d}}}{2}\right)s\left(\frac{\psi_{\mathrm{d}}}{2}\right) \\ c\left(\frac{\phi_{\mathrm{d}}}{2}\right)s\left(\frac{\theta_{\mathrm{d}}}{2}\right)c\left(\frac{\psi_{\mathrm{d}}}{2}\right) + s\left(\frac{\phi_{\mathrm{d}}}{2}\right)c\left(\frac{\theta_{\mathrm{d}}}{2}\right)s\left(\frac{\psi_{\mathrm{d}}}{2}\right) \\ c\left(\frac{\phi_{\mathrm{d}}}{2}\right)c\left(\frac{\theta_{\mathrm{d}}}{2}\right)s\left(\frac{\psi_{\mathrm{d}}}{2}\right) - s\left(\frac{\phi_{\mathrm{d}}}{2}\right)s\left(\frac{\theta_{\mathrm{d}}}{2}\right)c\left(\frac{\psi_{\mathrm{d}}}{2}\right) \end{bmatrix}, \quad (7)$$

where $s_{(\cdot)}$ and $c_{(\cdot)}$ are shorthand for $\sin(\cdot)$ and $\cos(\cdot)$, respectively.

4. Experiments

In this section, we demonstrate the results of our experiments. In particular, we show that the prototype discussed in Section 2.3 has successfully flown in a straight line at a constant altitude with manual control, while transitioning

Table 3. Gain parameters of the controllers.

Parameter	Value	Location
$\boldsymbol{K}_{\mathrm{p}}^{q}$	diag(6.5, 6.5, 2.8)	Eq. (2)
$\boldsymbol{K}_{\mathrm{p}}^{\omega}$	diag(0.06, 0.06, 0.06)	Eq. (4)
$\boldsymbol{K}_{\mathrm{i}}^{\omega}$	diag(0.08, 0.08, 0.02)	
$\boldsymbol{K}_{\mathrm{d}}^{\omega}$	diag(0.001, 0.001, 0)	

from the hover to forward flight mode with different tilt angles. All flight experiments were conducted indoors under windless conditions using the control system in **Fig. 5**. We implemented the control system in the flight computer (mRo PixRacer Pro) using MATLAB® and Simulink® with the UAV Toolbox Support Package for PX4 Autopilots [a]. The controller gains of the attitude controller Eq. (2) and the angular velocity controller Eq. (4) are given in **Table 3**. **Figs. 6(a)**, **(b)**, and **(c)** show the sequence images and the graphs of the ZYX-Euler angles ϕ, θ, ψ, desired pitch angle θ_{d}, and the desired total thrust f_{d} of the flight experiments at $\gamma = -45°$, 0°, and 45°, respectively. The desired roll angle ϕ_{d} and the desired yaw angle ψ_{d} are set at constant 0°, and the desired pitch angle θ_{d} and the desired total thrust f_{d} are given manually. Here, the desired pitch angle θ_{d} in $\mathcal{M}_{\mathrm{forward}}$ was set at approximately 70° to prevent the aircraft from crashing into a wall due to limited indoor space. Although there is a slight movement in altitude due to manual control, it can be observed that in all cases the proposed tailsitter achieved a smooth transition from hover to forward flight mode. Note also that different tilt angles give different staggers in $\mathcal{M}_{\mathrm{forward}}$; negative tilt angles (e.g., −45°) give negative wing stagger and positive tilt angles (e.g., 45°) give positive wing stagger.

5. Conclusion

In this study, we proposed a novel tailsitter UAV with configurable wings and developed its prototype. In experiments, we show that it can smoothly transition from the hover to forward flight mode with three wing configurations: non-staggered wings (biplane) and positively and negatively staggered wings (tandem wing plane), using the standard controllers for the conventional quadrotors.

The stagger angle of a biplane and tandem wing plane affects their aerodynamic characteristics [19, 20]. In particular, it has been shown that the maximum lift coefficient is greater with the positive stagger than with zero stagger. This finding motivates further investigation into the potential benefits of varying the stagger during flight. In future work, we will clarify how the aerodynamic characteristics change depending on the wing configuration for forward flight, and propose a dynamic desired tilt angle generator that maximizes its flight efficiency.

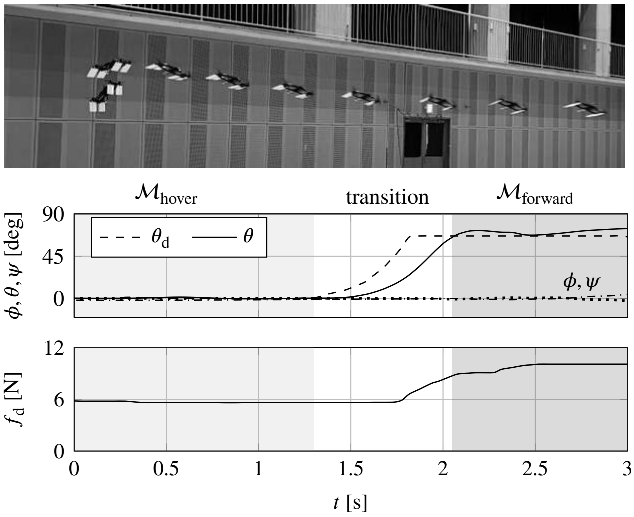

(a) Tilt angle $\gamma = -45°$

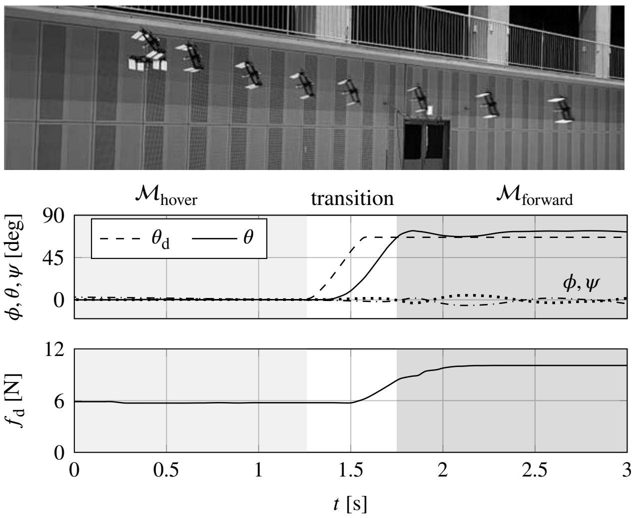

(b) Tilt angle $\gamma = 0°$

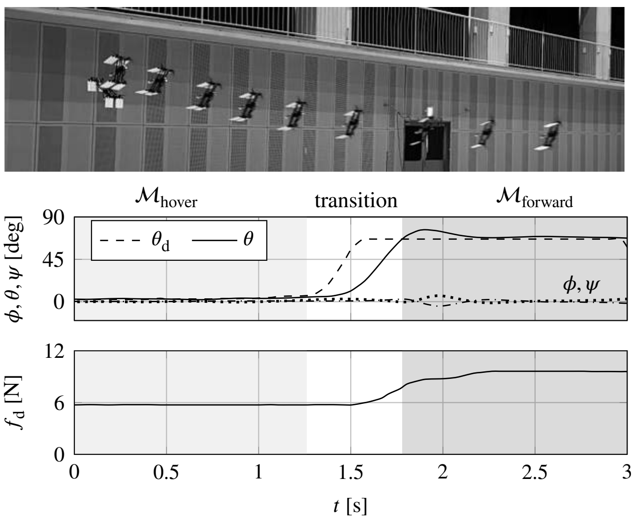

(c) Tilt angle $\gamma = 45°$

Fig. 6. Transition from $\mathcal{M}_{\mathrm{hover}}$ to $\mathcal{M}_{\mathrm{forward}}$ at fixed tilt angles.

References:

[1] B. Crowther, A. Lanzon, M. Maya-Gonzalez, and D. Langkamp, "Kinematic analysis and control design for a nonplanar multiro-

tor vehicle," J. Guid. Control Dyn., Vol.34, No.4, pp. 1157-1171, 2011. https://doi.org/10.2514/1.51186
[2] A. Sakaguchi, T. Takimoto, and T. Ushio, "A novel quadcopter with a tilting frame using parallel link mechanism," Int. Conf. Unmanned Aircr. Syst., pp. 674-683, 2019. https://doi.org/10.1109/ICUAS.2019.8797934
[3] K. Kawasaki, Y. Motegi, M. Zhao, K. Okada, and M. Inaba, "Dual connected bi-copter with new wall trace locomotion feasibility that can fly at arbitrary tilt angle," IEEE/RSJ Int. Conf. Intell. Robots Syst., pp. 524-531, 2015. https://doi.org/10.1109/IROS.2015.7353422
[4] P. Zheng, X. Tan, B. B. Kocer, E. Yang, and M. Kovac, "TiltDrone: A fully-actuated tilting quadrotor platform," IEEE Robot. Autom. Lett., Vol.5, No.4, pp. 6845-6852, 2020. https://doi.org/10.1109/LRA.2020.3010460
[5] M. Ryll, H. H. Bülthoff, and P. R. Giordano, "A novel overactuated quadrotor unmanned aerial vehicle: Modeling, control, and experimental validation," IEEE Trans. Control Syst. Technol., Vol.23, No.2, pp. 540-556, 2015. https://doi.org/10.1109/TCST.2014.2330999
[6] A. Oosedo et al., "Flight control systems of a quad tilt rotor unmanned aerial vehicle for a large attitude change," IEEE Int. Conf. Robot. Autom., pp. 2326-2331, 2015. https://doi.org/10.1109/ICRA.2015.7139508
[7] A. B. Junaid, A. D. D. C. Sanchez, J. B. Bosch, N. Vitzilaios, and Y. Zweiri, "Design and implementation of a dual-axis tilting quadcopter," Robotics, Vol.7, No.4, Article No.65, 2018. https://doi.org/10.3390/robotics7040065
[8] V. Riviere, A. Manecy, and S. Viollet, "Agile robotic fliers: A morphing-based approach," Soft Robot., Vol.5, No.5, pp. 541-553, 2018. https://doi.org/10.1089/soro.2017.0120
[9] A. Desbiez et al., "X-Morf: A Crash-separable quadrotor that morfs its X-geometry in flight," Workshop Res. Educ. Dev. Unmanned Aer. Syst., pp. 222-227, 2017. https://doi.org/10.1109/RED-UAS.2017.8101670
[10] D. Falanga, K. Kleber, S. Mintchev, D. Floreano, and D. Scaramuzza, "The foldable drone: A morphing quadrotor that can squeeze and fly," IEEE Robot. Autom. Lett., Vol.4, No.2, pp. 209-216, 2019. https://doi.org/10.1109/LRA.2018.2885575
[11] T. Fukuda, A. Sakaguchi, T. Takimoto, and T. Ushio, "Modeling and stabilization of the novel quadrotor with tilting propeller," 2016 Int. Symp. Nonlinear Theory Appl., pp. 173-176, 2016. https://doi.org/10.34385/proc.48.A3L-E-4
[12] A. Sakaguchi and K. Yamamoto, "A novel quadrotor with a 3-axis deformable frame using tilting motions of parallel link modules without thrust loss," IEEE Robot. Autom. Lett., Vol.7, No.4, pp. 9581-9588, 2022. https://doi.org/10.1109/LRA.2022.3191195
[13] V. Hrishikeshavan, C. Bogdanowicz, and I. Chopra, "Design, performance and testing of a quad rotor biplane micro air vehicle for multi role missions," Int. J. Micro Air Veh., Vol.6, No.3, pp. 155-173, 2014. https://doi.org/10.1260/1756-8293.6.3.155
[14] A. Oosedo, S. Abiko, A. Konno, and M. Uchiyama, "Optimal transition from hovering to level-flight of a quadrotor tail-sitter UAV," Auton. Robots, Vol.41, No.5, pp. 1143-1159, 2017. https://doi.org/10.1007/s10514-016-9599-4
[15] Z. Qiao et al., "A comprehensive design and experiment of a biplane quadrotor tail-sitter UAV," Drones, Vol.7, No.5, Article No.292, 2023. https://doi.org/10.3390/drones7050292
[16] D. D. North, R. C. Busan, and G. Howland, "Design and fabrication of the LA-8 distributed electric propulsion VTOL testbed," AIAA SciTech 2021 Forum, 2021. https://doi.org/10.2514/6.2021-1188
[17] J. Winslow, H. Otsuka, B. Govindarajan, and I. Chopra, "Basic understanding of airfoil characteristics at low Reynolds numbers (10^4–10^5)," J. Aircr., Vol.55, No.3, pp. 1050-1061, 2018. https://doi.org/10.2514/1.C034415
[18] D. Brescianini, M. Hehn, and R. D'Andrea, "Nonlinear quadrocopter attitude control," Technical Report, Institute for Dynamic Systems and Control, ETH Zürich, 2013. https://doi.org/10.3929/ethz-a-009970340
[19] J.-M. Moschetta and C. Thipyopas, "Aerodynamic performance of a biplane micro air vehicle," J,. Aircr., Vol.44, No.1, pp. 291-299, 2007. https://doi.org/10.2514/1.23286
[20] H. Kang, N. Genco, and A. Altman, "Empirically derived biplane lift as a function of gap and stagger," J. Aircr., Vol.50, No.1, pp. 292-298, 2013. https://doi.org/10.2514/1.C031111

Supporting Online Materials:

[a] MathWorks®, "PX4 Autopilot Support from UAV Toolbox." https://jp.mathworks.com/hardware-support/px4-autopilots.html [Accessed December 15, 2023]

Name:
Shunsuke Yoshinaga

Affiliation:
Master's Student, Graduate School of Information Science and Electrical Engineering, Kyushu University

Address:
744 Motooka, Nishi-ku, Fukuoka, Fukuoka 819-0395, Japan

Brief Biographical History:
2018- Undergraduate Student, Kyushu University
2022- Graduate Student, Kyushu University

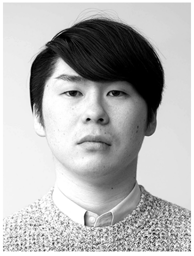

Name:
Akinori Sakaguchi

ORCID:
0000-0003-1895-9570

Affiliation:
Assistant Professor, Faculty of Information Science and Electrical Engineering, Kyushu University

Address:
744 Motooka, Nishi-ku, Fukuoka, Fukuoka 819-0395, Japan

Brief Biographical History:
2021 Received Ph.D. degree from Osaka University
2021- Postdoctoral Researcher, Kyushu University
2022- Project Assistant Professor, Kyushu University
2023- Assistant Professor, Kyushu University

Main Works:
• "A novel quadrotor with a 3-axis deformable frame using tilting motions of parallel link modules without thrust loss," IEEE Robot. Autom. Lett., Vol.7, No.4, pp. 9581-9588, 2022.

Membership in Academic Societies:
• Institute of Electrical and Electronics Engineers (IEEE)
• The Robotics Society of Japan (RSJ)
• The Japan Society of Mechanical Engineers (JSME)
• The Society of Instrument and Control Engineers (SICE)

Name:
Kaoru Yamamoto

ORCID:
0000-0003-1888-3529

Affiliation:
Associate Professor, Faculty of Information Science and Electrical Engineering, Kyushu University

Address:
744 Motooka, Nishi-ku, Fukuoka, Fukuoka 819-0395, Japan

Brief Biographical History:
2016 Received Ph.D. degree from University of Cambridge
2016- Postdoctoral Researcher, University of Minnesota Twin Cities
2017- Postdoctoral Researcher, Lund University
2018- Associate Professor, Kyushu University

Main Works:
• "Bounded disturbance amplification for mass chains with passive interconnection," IEEE Trans. Autom. Control, Vol.61, No.6, pp. 1565-1574, 2016.

Membership in Academic Societies:
• Institute of Electrical and Electronics Engineers (IEEE)
• The Society of Instrument and Control Engineers (SICE)
• The Robotics Society of Japan (RSJ)